Particle-phase diffusion modulates partitioning of semivolatile organic compounds to aged secondary organic aerosol

Rahul A. Zaveri, [1,*] *John E. Shilling,*[1] *Alla Zelenyuk,*[1] *Maria A. Zawadowicz,*[1] *Kaitlyn Suski,*[1,§]

Swarup China,[2] *David M. Bell,*[1,‡] *Daniel Veghte,*[2,†] *and Alexander Laskin*[3]

[1]Atmospheric Sciences and Global Change Division, Pacific Northwest National Laboratory, Richland, WA 99352, United States

[2]William R. Wiley Environmental Molecular Sciences Laboratory, Pacific Northwest National Laboratory, Richland, WA 99352, United States

[3]Department of Chemistry, Purdue University, West Lafayette, IN 47907, United States

KEYWORDS: Biogenic secondary organic aerosol, gas-particle partitioning, aerosol dynamics, semisolid phase state, viscosity, bulk diffusivity

ABSTRACT: Diffusivity of semivolatile organic compounds (SVOCs) in the bulk particle phase of viscous atmospheric secondary organic aerosol (SOA) can have profound impacts on aerosol growth and size distribution dynamics. Here we investigate the bulk diffusivity of SVOCs formed from photooxidation of isoprene as they partition to a bimodal aerosol consisting of an Aitken (potassium sulfate) and accumulation mode (aged α-pinene SOA) particles as a function of relative humidity (RH). Model analysis of the observed size distribution evolution shows that liquid-like diffusion coefficient values of $D_b > 10^{-10}$ cm^2 s^{-1} fail to explain the growth of the Aitken mode. Instead, much lower values of D_b between 2.5 X 10^{-15} cm^2 s^{-1} at 32% RH and 8 X 10^{-15} cm^2 s^{-1} at 82% RH were needed to successfully reproduce the growth of both modes. Diffusivity within aged α-pinene SOA remains appreciably slow even at 80% RH, resulting in hindered partitioning of SVOCs to large viscous particles and allowing smaller and relatively less viscous particles to effectively absorb the available SVOCs and grow much faster than would be possible otherwise. These results have important implications for modeling SOA formation and growth in the ambient atmosphere.

TOC/ABSTRACT ART

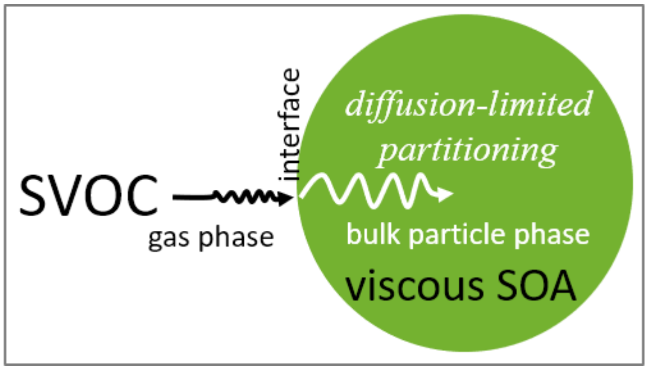

INTRODUCTION

Atmospheric aerosols play an important role in the Earth's radiative balance and climate.[1] Of the many different chemical components, organic compounds constitute a major fraction of the submicron aerosol mass.[2, 3] While combustion of fossil fuel and biomass burning directly emit organic aerosol (OA), the global budget is dominated by secondary organic aerosols (SOA) that form in the atmosphere via gas-particle partitioning of oxidation products of volatile organic compounds (VOCs) of both anthropogenic and biogenic origins.[2-4] Anthropogenic activities emit thousands of VOCs, [5-7] but biogenic VOCs account for about 90% of the emission total, [8] with isoprene and monoterpenes dominating the global non-methane BVOC emission budget [9-11]. Besides contributing to the total aerosol mass, SOA formation plays a crucial role in the growth of pre-existing ultrafine particles to larger sizes at which they can act as cloud condensation nuclei.[12-14] Consequently, it is important for aerosol-climate models to be able to accurately predict SOA mass and its size distribution, which depend on the complex interplay between the kinetics and thermodynamics of gas-particle partitioning.[15, 16]

For a given aerosol loading, gas-particle partitioning is driven by Raoult's law and the timescale of partitioning mainly depends on the particle diameter (D_p), the volatility (i.e., the effective saturation vapor pressure, C*) of the condensing compound, its gas-phase diffusivity (D_g), its mass accommodation coefficients (α) on the pre-existing particle surface, and its particle-phase bulk diffusivity (D_b).[16, 17] Extremely low-volatility organic compounds (ELVOCs, $C^* < 10^{-3}$ μg m^{-3}) kinetically condense on pre-existing aerosol particles according to the Fuchs-corrected surface area size distribution.[18, 19] In this case, the partitioning is effectively irreversible, and the condensation timescale is controlled by particle size, gas-phase diffusion and mass accommodation on the surface, while bulk diffusion is irrelevant. Consequently, SOA formation from ELVOCs facilitates the growth of the smallest pre-existing particles.[12, 19, 20] In contrast, semivolatile organic compounds (SVOCs, $10^{-1} < C^* < 10^{2}$ μg m^{-3}) tend to partition according to the pre-existing organic mass size distribution at thermodynamic equilibrium. In Raoult's law-based partitioning, the pre-existing organic aerosol mass serves as a solvent into which the SVOCs are absorbed to form an ideal mixture. As a result, SOA formation from SVOCs generally favors the growth of the largest pre-existing particles.[12, 19, 21] Representing all of the SOA formed in atmospheric models with either the kinetic approach or the mass-based equilibrium approach dramatically alters the aerosol size distribution and have a large impact on the simulated aerosol radiative effects.[22]

If the absorbing particulate organic phase is liquid-like (i.e., $D_b > 10^{-10}$ cm^2 s^{-1}), then the bulk diffusion timescales are < 1 s for submicron-sized particles and gas-particle equilibrium is quickly reached across the size distribution. Most atmospheric models currently assume liquid organic particles with instantaneous equilibration of SVOCs.[23] However, there is mounting evidence from laboratory and field observations that SOA may exist as viscous semisolids with low bulk diffusivity ($D_b < 10^{-13}$ cm^2 s^{-1}) under dry to moderate relative humidity (RH) and gradually transition to a liquid-like state at high RH.[24-39] The high viscosity and the associated semisolid phase state are thought to be caused by oligomers formed from accretion reactions amongst some SVOCs or "monomers" after partitioning into the pre-existing organic aerosol.[28, 29, 40-43] The oligomers have relatively large molecular weights and are effectively nonvolatile at ambient temperatures. Low bulk diffusivity inside viscous semisolid particles slows gas-particle partitioning[34, 44-47], and it may take several hours to days for SVOCs to equilibrate with particles across the entire size distribution.[16, 17, 48] Furthermore, if the SVOCs react within the particle phase to form oligomers, the expected equilibrium partitioning across the size distribution may never be reached within the atmospheric lifetime of the SOA particles. While an increase in RH increases the extent of evaporation[38, 46, 49] and facilitates inter-particle mixing processes[50] in some freshly formed SOA systems, the effects of RH on the growth kinetics of aged SOA is yet poorly understood.

In a previous study, we probed the effects of bulk diffusion by observing particle size distribution evolution resulting from isoprene SOA formation under dry conditions (RH < 2%) in the presence of bimodal seed aerosol consisting of an Aitken mode composed of ammonium sulfate and an accumulation mode composed of aged α-pinene SOA.[34] We found that low bulk diffusivity (D_b = 2 X 10^{-15} cm^2 s^{-1}) inside the dry α-pinene SOA hindered the partitioning of SVOCs formed from isoprene photooxidation into the accumulation mode, which allowed significantly higher amounts of SVOCs to partition to the Aitken mode particles than would have been possible if the accumulation mode SOA was liquid-like. However, α-pinene SOA is expected to become less viscous as the RH increases due to the plasticizing effect of liquid aerosol water[27], which can potentially lower the gas-particle equilibration timescale and alter size-dependent growth kinetics. In this follow up study, we report results from a laboratory chamber investigation of SOA growth kinetics using the same experimental strategy as before[34] but conducted under different RH conditions ranging from 32% to 82%.

EXPERIMENTAL SECTION

Growth Experiments. A series of six SOA growth kinetics experiments were conducted at 23-25 °C under low-NO_x conditions with RH ranging from 32% to 82% in 10.6 m^3 Fluorinated Ethylene Propylene (FEP) Teflon environmental chamber at Pacific Northwest National Laboratory[34, 51]. The chamber was continually flushed with purified air prior to the start of each experiment until particle number concentrations <10 cm^{-3} were recorded with a Scanning Mobility Particle Sizer (SMPS). The experiments were run in the batch mode in which the reactants were injected into the chamber in discrete quantities.

Each experiment consisted of two stages. In stage 1, α-pinene was injected into the chamber either by evaporating a measured quantity of liquid under a stream of pure air. Hydrogen peroxide (50%, Aldrich) was evaporated into the chamber by gently warming the liquid under a flow of pure air and served as an OH radical precursor. RH was measured with a Rotronics sensor (SC-05) located inside the chamber. Solid potassium sulfate (K_2SO_4) seed particles of 50 nm diameter were injected into the chamber by drying atomized aqueous solution of K_2SO_4 and size-selecting them with a DMA (TSI, 3080L). K_2SO_4 (instead of ammonium sulfate) was used here because of its high deliquescence RH of 96%[52] to avoid any contribution to aerosol liquid water from the inorganic seed. Photochemistry was initiated by turning on 104 UV-blacklights (Q-labs, UV-340) symmetrically surrounding the chamber that produced a stable UV flux equivalent to a photolysis rate of $J_{NO2} = 2.7 \times 10^{-3}$ s^{-1} and $J_{H2O2} \sim 4.7 \times 10^{-5}$ s^{-1}. Photooxidation of α-pinene with OH radicals formed SOA on the K_2SO_4 seed particles immediately after the UV lights were turned on. The UV lights were briefly turned off after about 1.5 to 3 h when the particles had grown to about 200 nm. Two size-selected samples of the freshly formed α-pinene

SOA ("P_{fresh}") were dried and then transferred into separate small chambers to study their evaporation kinetics[25] at room temperature under dry (RH < 5%) and humid (RH = 75%) conditions.[38] More α-pinene and H_2O_2 were added into the chamber as necessary and the UV lights were turned on again to continue the growth of the α-pinene SOA to about 300-400 nm (accumulation mode) and photochemically age it for about 16 h during which time α-pinene was almost completely consumed. The UV lights were turned off and another set of two size-selected samples of the aged α-pinene SOA particles ("P_{aged}") were dried and then transferred into separate small chambers to study their evaporation kinetics at room temperature under dry and humid conditions. Toward the end of stage 1, isoprene and Aitken mode K_2SO_4 seed (D_p = 40 nm) were injected into the environmental chamber in the presence of aged α-pinene SOA. Then in stage 2 of the experiment, the UV lights were turned on to form isoprene SOA on the pre-existing bimodal aerosol. Based on the modeled decay of isoprene, the OH concentration during stage 2 ranged between 1.8×10^{-6} and 2.4×10^{-6} molecule cm^{-3}.

Isoprene and α-pinene mixing ratio and their selected oxidation products were measured in real time with a Proton Transfer Reaction Mass Spectrometer[53] (PTR-MS; Ionicon high-sensitivity). The PTR-MS was regularly calibrated during the experimental work using a cylinder of known gas concentrations. Particle size distributions were measured continuously using an SMPS (TSI, 3936). The SMPS data were recorded with a time resolution of 5 min, and the instrument was set to measure particles in the range 14–710 nm mobility diameter divided into 110 logarithmically distributed size bins. Data were processed with standard TSI software including a correction for multiple-charged particles. The SOA mass concentrations reported here were calculated from SMPS volume using a density of 1.4 g cm^{-3}.

At the end of each experiment, an aerosol sample taken from the environmental chamber was collected onto the Teflon filter for offline analysis. The SOA sample was probed directly from the filter using a custom-built Nanospray Desorption Electrospray Ionization (Nano-DESI) source coupled to a high resolution LTQ-Orbitrap mass spectrometer[54, 55] (Thermo Electron, Bremen, Germany). A more detailed description of Nano-DESI-HRMS is given in the Supporting Information.

Evaporation Experiments. In each experiment, freshly formed and aged α-pinene SOA samples (P_{fresh} and P_{aged}) were size-selected with a differential mobility analyzer (DMA, TSI Inc., Model 3081), passed through two charcoal denuders (TSI Inc., Model 3062) connected in series and kept at room temperature to remove gas-phase organics, and loaded into one of the evaporation chambers (volumes of 7, 11, or 13 L) that were partially filled with activated charcoal to continuously remove the evaporated organics.[25] Both P_{fresh} and P_{aged} samples were evaporated at room temperature under dry (RH <5%) and humid (75% RH) conditions.[38]

The typical duration of the evaporation experiments was ~24 hours, during which particle vacuum aerodynamic diameter (D_{va}), shape, density, and composition were periodically measured using the single particle mass spectrometer, miniSPLAT[56] (a brief description is provided in the Supporting Information). Particle evaporation kinetics, expressed as organic volume fraction remaining (VFR) as a function of time, was quantified by measuring changes in D_{va}, with 0.5% precision, taking into account the contribution of solid K_2SO_4 seeds. While the particle number concentration in the evaporation chamber decreases from ~100 cm^{-3} to 2-5 cm^{-3} due to wall losses and periodic sampling over 24 hours, these losses had no effect on the evaporation rates, which were determined from the measured changes in particles D_{va}.

Box Model. The sectional aerosol box model version of Model for Simulating Aerosol Interactions and Chemistry (MOSAIC)[16, 57] was used to interpret the observed bimodal aerosol growth kinetics. MOSAIC dynamically partitions multiple compounds to all particle size bins by considering compound volatility (C*), gas-phase diffusion (D_g), interfacial mass accommodation (α), intra-particle bulk diffusion (D_b), and reversible particle-phase reactions. The thermodynamic driving force for mass transfer of semivolatile compounds is governed by Raoult's law, while their bulk diffusion within the particle is treated using the two-film theory[16]. A more detailed description of the dynamic gas-particle partitioning treatment in MOSAIC is given in the Supporting Information.

RESULTS AND DISCUSSION

Bimodal Aerosol Growth Kinetics. Each chamber experiment was about 30 h long and consisted of two stages. Stage 1, which typically took about 26 h, focused on preparing a bimodal aerosol composed of aged α-pinene SOA accumulation mode and solid K_2SO_4 Aitken mode. In stage 2, this bimodal aerosol could grow via additional SOA formation from photooxidation of isoprene. As an illustrative example, the time evolution of T, RH, α-pinene, isoprene, and total particle number and volume concentrations for one experiment is shown in Figure 1a. The associated number size distribution evolution is shown in Figure 1b. In this experiment, the RH was about 35% when the UV lights were off and decreased to ~30% due to increase in temperature when the UV lights were turned on, with an average of ~32±1.1% during stage 2. The α-pinene SOA accumulation mode rapidly grew within 2 h after the UV lights were turned on during stage 1. After brief interruption at the time when the freshly formed α-pinene SOA particles were sampled for evaporation kinetics study, the accumulation mode continued to grow for ~10 h to 385.4 nm until α-pinene was completely consumed and remained at that size while it continued to photochemically age for another ~7 h. Although the aged α-pinene SOA accumulation mode experienced a two-fold dilution (as seen from the decrease in the total particle volume concentration) when the UV lights were turned off during the injections of 40 nm solid K_2SO_4 particles and isoprene, its size remained nearly constant despite a concurrent factor of two reduction in the gas phase concentration of α-pinene SOA species, suggesting that the aged α-pinene SOA was quite viscous and/or composed of low volatility compounds.

During isoprene SOA formation in stage 2, the ~40 nm Aitken mode grew to 101 nm in 90 min while the accumulation mode grew from 385 nm to 414 nm. In terms of mass, about 1.3 μg m^{-3} of isoprene SOA condensed on the Aitken mode seed, while 8.7 μg m^{-3} of isoprene SOA was added to the pre-existing 30.4 μg m^{-3} of aged α-pinene SOA. Similar bimodal growth behavior was observed in the other five experiments carried out at higher RH as summarized in Table 1. In each experiment, irrespective of the RH, the aged α-pinene SOA accumulation mode received >80% of the total isoprene SOA formed while the remaining <20% condensed on the Aitken mode. The physicochemical mechanism of SOA formation is reflected in the characteristics of the bimodal aerosol size distribution evolution, which we use in conjunction with the dynamic gas-particle partitioning model MOSAIC to unravel the complex interplay between kinetics and thermodynamics.

Aged α-pinene SOA Seed. Before interpreting the growth kinetics of the aged α-pinene SOA, it is worth contrasting its volatility against that of the freshly formed α-pinene SOA. Figure 2 shows evaporation kinetics of both freshly formed and aged α-pinene SOA for three selected experiments in which the α-pinene SOA was formed at 32%, 43%, and 82% RH. The freshly formed and aged α-pinene SOA from each experiment were allowed to evaporate under dry (RH < 5%) and humid (75% RH) conditions. In the case of freshly formed SOA formed under three different RH conditions, less than 30% of the organic volume fraction remained after 6 h of evaporation at 75% RH (Figure 2a). In comparison, all three freshly formed SOA samples evaporated appreciably slower under dry conditions after first 2 h, with more than 40% of the organic volume fraction remaining after 5 h. These results clearly indicate that freshly formed α-pinene SOA was highly viscous under dry conditions, which slowed down the diffusion of semivolatile species from the bulk of the particle to the surface inhibiting their evaporation. The viscosity was markedly lower for evaporation at 75% RH as indicated by the greater amounts of semivolatile species that were able to evaporate at a faster rate. These results are consistent with previously reported direct measurements of viscosity of freshly formed α-pinene SOA as a function of RH.[27, 33]

In stark contrast, the aged α-pinene SOA samples from all three experiments evaporated at similar rates and to similar extents under both dry (RH < 5%) and humid (RH = 75%) conditions, with more than 40% of the organic volume fraction remaining after 22 h (Figure 2b), suggesting a significant loss of semivolatile particle species during aging. The slightly slower evaporation of the remaining semivolatile species during evaporation at 75% can be attributed to their lower effective vapor pressures in the presence of particle-phase liquid water that acts as a solvent in Raoult's law-based partitioning. Furthermore, these evaporation profiles are remarkably similar to those for aged α-pinene SOA formed and evaporated under dry conditions (i.e., RH < 5%) in terms of both the evaporation rates and extents. These results thus suggest that aged α-pinene SOA may remain highly viscous even as the RH increases up to 75% or higher.

Figure 3a shows the nano-DESI-HRMS spectra of the bulk SOA samples collected at the end of stage 2 for the three experiments at 32%, 45%, and 82% RH. Although these samples include isoprene SOA, the bulk was still dominated by aged α-pinene SOA at 65-75% of the total organic mass (Table 1). These spectra qualitatively indicate the presence of high molecular weight oligomers, with relative abundances of respectively 56%, 58%, and 69% at 32% RH, 45% RH and 82% RH, which likely caused high viscosity over the full range of RH considered in this study. HRMS data were further processed using a suite of Microsoft Excel macros, including background subtraction, first and second order mass defect analysis, and grouping homologous peaks.[58] Elemental formula for each group was assigned using the MIDAS molecular formula calculator. The molecular corridor approach of Li et al.[59] was then applied to estimate volatility as shown in Figure 3b. Relatively less volatile α-pinene SOA species were formed at 82% RH compared to lower RH levels (assuming the ionization and detection efficiencies are similar in all samples), consistent with relatively slower evaporation observed at high RH (shown in Figure 2a). In a previous study, Kidd et al.[28] found that the contribution from higher molecular mass products in SOA formed from ozonolysis of α-pinene decreased with increase in the formation RH, accompanied by a decrease in viscosity. In contrast, α-pinene SOA in the present study was formed from OH oxidation, which may be cause for the differences in the observed compositional trends with RH.

Model Interpretation of Growth Kinetics. Photooxidation of isoprene forms many products, some of which lead to SOA formation.[60] In the presence of non-aqueous aerosol seed and low-

NO_x conditions, as is the case here, SOA efficiently forms via partitioning of isoprene dihydroxydihydroperoxide ($C_5H_{12}O_6$) and a suite of related multifunctional organic peroxides, some of which form oligomers via particle-phase reactions.[34, 61-63] In our previous bimodal aerosol growth kinetics study conducted under dry conditions, about 50% of isoprene SOA mass was found to be composed of $C_5H_{12}O_5$ and $C_5H_{12}O_6$ while the balance was inferred to be oligomers formed from particle-phase reactions of SVOCs.[34] Both evaporation and growth kinetics of this SOA could be reproduced only when a low value for bulk diffusion coefficient of $D_b = 2 \times 10^{-15}$ cm^2 s^{-1} (i.e., the "semisolid scenario") was considered in the model. The complex mixture of oligomers was approximated in the model as two surrogate nonvolatile dimers – $Dimer_1$ and $Dimer_2$, each reversibly formed from respective surrogate monomers – $SVOC_1$ and $SVOC_2$, with the same formation rate constant (k_f) but different decomposition constants ($k_{d,1}$ and $k_{d,2}$):

$$SVOC_1 + SVOC_1 \underset{k_{d,1}}{\overset{k_f}{\rightleftarrows}} Dimer_1 \text{ ,and} \qquad (1)$$

$$SVOC_2 + SVOC_2 \underset{k_{d,2}}{\overset{k_f}{\rightleftarrows}} Dimer_2 , \qquad (2)$$

The estimated rate constants were $k_f = 3 \times 10^{-6}$ m^3 mol^{-1} s^{-1}, $k_{d,1} = 5 \times 10^{-4}$ s^{-1} and $k_{d,2} = 1.4 \times 10^{-5}$ s^{-1}, and the estimated C* values for $C_5H_{12}O_5$ and $C_5H_{12}O_6$, $SVOC_1$, and $SVOC_2$ were 2, 2, 30, and 30 μg m^{-3}, respectively. Both SVOCs and their dimers were assumed to have molecular weights of 136 g mol^{-1} and 272 g mol^{-1}, respectively.

Here we use the same set of rate constants, C* values, and compositional constraints in MOSAIC to determine the values of D_b that can reproduce the observed bimodal aerosol growth kinetics at different RH. In addition to the semisolid scenario, we simulate the growth kinetics with two "liquid-like" scenarios (i.e., $D_b > 10^{-10}$ cm^2 s^{-1})—one with completely miscible isoprene and α-pinene SOA (corresponding to activity coefficients of isoprene SVOCs equal to unity in α-pinene SOA), and another with completely immiscible isoprene and α-pinene SOA (corresponding to activity coefficients of isoprene SVOCs in α-pinene SOA equal to 10000). We also simulate the growth kinetics with the "nonvolatile" scenario in which SOA formation is assumed to occur entirely from condensation of a nonvolatile vapor (i.e., $C^* = 0$ μg m^{-3}). The nonvolatile scenario also represents the rapid reactive uptake mechanism that results in nearly identical size distribution evolution.[64] Isoprene mixing ratio and aerosol size distribution in the model were initialized using observations at the beginning of stage 2. The Aitken mode was initialized as an inert solid representing K_2SO_4, while the accumulation mode composed of α-pinene SOA (with a 50 nm inert solid core) was assumed to be composed of a nonvolatile organic compound with a molecular weight of 250 g mol^{-1} for the purpose of kinetically partitioning isoprene SOA into it as governed by Raoult's law. Furthermore, RH-dependent hygroscopicities for semisolid α-pinene SOA and isoprene SOA were used to calculate aerosol water content as a function of RH[65, 66], with the option of including or excluding the aerosol water as a solvent in Raoult's law-based partitioning. In the case where water is included in Raoult's law, the model assumes ideal mixing between water and organics. The OH radical concentration in the model was tuned to reproduce the observed decay of isoprene in the chamber. Although it takes several oxidation steps to produce the condensable oxidation products from isoprene photooxidation, the isoprene + OH reaction in the model was parameterized to directly form $C_5H_{12}O_5$, $C_5H_{12}O_6$, $SVOC_1$, and $SVOC_2$. The gas-phase yields of these four compounds were adjusted such that $C_5H_{12}O_5$, $C_5H_{12}O_6$, $SVOC_1$ + $Dimer_1$, and $SVOC_2$ + $Dimer_2$ respectively constituted 21%, 28%, 29%, and 22% of the newly formed isoprene SOA mass as previously modeled under dry conditions.[34] The mass accommodation coefficient α for the condensing vapors was set to 0.1. Particle wall loss was included in the model by constraining the predicted number concentration to that observed, while the total amount of isoprene SOA formed in the model was constrained by matching the predicted volume concentration to that observed after 90 min. This modeling approach effectively circumvents the uncertainties associated with gas-phase multigenerational photochemistry of isoprene and the yields of condensable oxidation products and their vapor wall losses.

Figure 4 shows the observed and modeled aerosol number size distributions after 90 min of isoprene SOA growth in stage 2 for four selected experiments conducted at average RH values of 32%, 43%, 74%, and 82%. Here, the predicted aerosol water was included as a solvent in each size bin for the liquid-like as well as semisolid scenarios, with the underlying rationale that diffusion of small molecules such as water is not kinetically limited on timescales of 1 s even for semisolid SOA.[67] In all experiments, the miscible liquid-like scenario appears to reproduce the size of the accumulation mode particles, but severely under-predicted the growth of the Aitken mode. In the absence of appreciable bulk diffusion limitation, the miscible liquid-like scenario tends to partition the condensing semivolatile organic vapors according to the pre-existing organic mass size distribution. As a result, the miscible liquid-like scenario partitioned more isoprene SOA than observed to the accumulation mode at the expense of the Aitken mode. The immiscible liquid-like scenario appears to improve the growth of the Aitken mode but still underpredicts it compared to the observed growth, especially in the low RH experiments.

However, this improvement is likely fortuitous because it requires complete immiscibility between the two SOA phases in the accumulation mode, corresponding to unrealistically high activity coefficients of isoprene SVOCs in the aged α-pinene SOA over the entire RH range considered here. Even a modest miscibility resulting from realistic activity coefficients between the two SOA phases would tend to decrease the predicted growth of the Aitken mode compared to the extreme case of the completely immiscible liquid-like scenario. The nonvolatile scenario performed better than the miscible liquid-like scenario with respect to matching the observed growth of the Aitken mode, but still underpredicted the growth of the Aitken mode. A nonvolatile vapor or a highly reactive semivolatile vapor condenses according to the pre-existing Fuchs-corrected surface area size distribution and thereby favors the growth of the smallest particles in terms of its diameter growth per unit time, although not necessarily in terms of its mass growth per particle per unit time. Thus, the nonvolatile scenario represents the maximum possible growth of the Aitken mode within the conventional modeling framework, but it still failed to explain the observations at all RH conditions considered here.

In contrast, the miscible semisolid scenario was able to reproduce the growth of both Aitken and accumulation modes when the D_b values for accumulation mode were set to values ranging from 2.5×10^{-15} cm^2 s^{-1} at 32% RH to about 8.5×10^{-15} cm^2 s^{-1} at high RH. These results suggest that the aged α-pinene SOA remained more viscous than peanut butter[68] even as the RH increased up to 82%, consistent with its evaporation kinetics behavior at 75% RH discussed earlier. In comparison, an order of magnitude larger value of D_b was consistently required for the freshly formed isoprene SOA in the Aitken mode. The higher diffusivity in the Aitken mode appears to be consistent with the relatively less volatile $C_5H_{12}O_5$ and $C_5H_{12}O_6$ initiating a liquid-like organic phase on the solid K_2SO_4 Aitken mode particles and facilitating the partitioning of more volatile SVOCs, which subsequently formed oligomers, leading to a modest decrease in the diffusivity due to limited aging (90 min).[34] At the same time, isoprene SOA is 2 to 3 times more hygroscopic than α-pinene SOA as RH increases,[66] which likely results in relatively higher diffusivity for the Aitken mode, with D_b values as high as 1×10^{-13} cm^2 s^{-1} at high RH. Similarly, the remaining two experiments carried out at ~45% and ~73% RH respectively required D_b values of 4.3×10^{-15} and 1×10^{-14} cm^2 s^{-1} for the accumulation mode and an order of magnitude larger values for the Aitken mode. It is worth noting here that the bulk diffusion treatment based on the two-film theory in MOSAIC assumes that D_b is constant within a given particle. Since the actual value of D_b depends on particle composition, there may be a gradient in D_b as the composition changes along the radius of the particle. The D_b values estimated here should therefore be regarded as effective bulk diffusion coefficients. For example, recent studies suggest that, in addition to particle phase state, viscous surface crust formation can affect SOA partitioning and multiphase reactivity.[69-71] The low effective D_b values required at high RH in the present study may indeed represent a viscous surface crust in aged α-pinene SOA as opposed to the entire bulk that may be relatively less viscous.

Figure S2 illustrates the sensitivity of the predicted growth kinetics to the prescribed D_b values. Using the same high value (i.e., the value required for the Aitken mode) for both aerosol modes significantly slows down the growth of the Aitken mode. Using the same low value (i.e., the value required for the accumulation mode) for both modes greatly speeds up the growth of the Aitken mode but still underpredicts it compared to the observation. As stated earlier, the mass accommodation coefficient (α) in the above simulations was set to 0.1. A recent study by Liu et al.[72] suggests that the value of α may be near-unity. To investigate its impact, additional sensitivity simulations were performed using α = 1. While the semisolid scenario was still able to reproduce the growth of both modes (using the nearly the same sets of D_b values that were used for α = 0.1), the height of the predicted Aitken mode was consistently much lower than observed (Figure S3), suggesting that the value of α may be closer to 0.1 than unity in our experiments. The overall performance of the miscible liquid-like scenario remained largely unchanged at low RH and significantly worsened at high RH when α = 1.

Growth of both aerosol modes could be reproduced when aerosol water was excluded as a solvent. In this case, the required D_b values for the accumulation mode ranged between 2×10^{-15} $cm^2\ s^{-1}$ and 4×10^{-15} $cm^2\ s^{-1}$, with no significant trend as a function of RH. Sensitivity of D_b to the volatility of the condensing compounds was also examined. For either of the aerosol water options in the Raoult's law calculations, the growth of both modes could be reproduced when about 90% of the newly formed isoprene SOA was assumed to be composed of $SVOC_1$ + $SVOC_2$ (C^* = 30 μg m^{-3}) and their dimers while the remaining 10% was in the form of $C_5H_{12}O_5$ + $C_5H_{12}O_6$ (C^* = 2 μg m^{-3}). In these cases, the D_b values required for the accumulation mode were about 20 to 40% higher than the base composition simulations.

Figure 5 summarizes the variation of D_b in aged α-pinene SOA as a function of RH for the different semisolid scenario assumptions for all six experiments along with the one conducted previously under dry conditions. If water is excluded from the solvent mass, we find no trend in D_b as a function of RH. However, if aerosol water does serve as a solvent for absorbing SVOCs according to Raoult's law, then the estimated D_b increases by only about a factor of five as the RH increases from <2% to 80% and the RH-dependence appears to be non-linear. In comparison, an increase of nearly three orders of magnitude over the same RH range is expected for freshly formed α-pinene.[27, 33] Additional work focused on the direct measurements of viscosity and diffusivity for aged SOA from different precursors is needed to confirm the significant diffusion limitation inferred for aged α-pinene SOA in this study.

These results have important implications for aerosol growth in the atmospheric environment where the accumulation mode SOA particles can age for several days before they are removed by dry or wet deposition. In contrast, nucleation and Aitken mode particles have much shorter lifetimes and are typically composed of freshly formed SOA that may be less viscous or even liquid-like at high RH. Thus, the hindered growth of the aged accumulation mode SOA would allow the smaller particles to effectively absorb the available SVOCs and grow much faster than would be possible otherwise. If these SVOCs undergo particle-phase reactions to form low volatility oligomers, as is the case in the present study, then the small particles will continue to absorb the SVOCs and grow at the expense of larger particles. Although formation of oligomers in small particles would gradually increase their viscosity, they can still continue to absorb the SVOCs owing to much shorter bulk diffusion time scales compared to large particles (bulk diffusion time scales varies as D_p^2).[34] This process would facilitate the growth of freshly nucleated particles to the accumulation mode and thereby increase their lifetime in the atmosphere and their ability to serve as CCN.

Table 1. Summary of Aerosol Growth Experiments.

		Initial (at the beginning of stage 2)				After 90 min growth in stage 2 from isoprene SOA formation				
		Aitken Mode (solid K_2SO_4)		Accumulation Mode (aged α-pinene SOA)			Aitken Mode		Accumulation Mode	
Expt.	RH (%) Mean±SD	D_p (nm)	SOA (μg m^{-3})	D_p (nm)	SOA (μg m^{-3})	Δisoprene (ppbv)	D_p (nm)	ΔSOA (μg m^{-3})	D_p (nm)	ΔSOA (μg m^{-3})
1	32±1.1	40	0	385.4	30.4	20.8	101.8	1.3	414.2	8.7
2	43.0±1.3	40	0	445.1	42.0	35.0	121.9	1.6	495.8	12.7
3	45.2±1.7	40	0	399.6	21.8	22.1	115.1	1.4	445.5	7.6
4	72.7±3.2	40	0	371.8	22.6	40.7	117.6	1.8	414.2	10.2
5	74.0±3.6	40	0	289.0	16.3	22.2	101.8	0.9	333.8	6.8
6	82.0±1.3	40	0	310.6	18.4	25.4	109.4	1.5	368.9	6.2

FIGURES

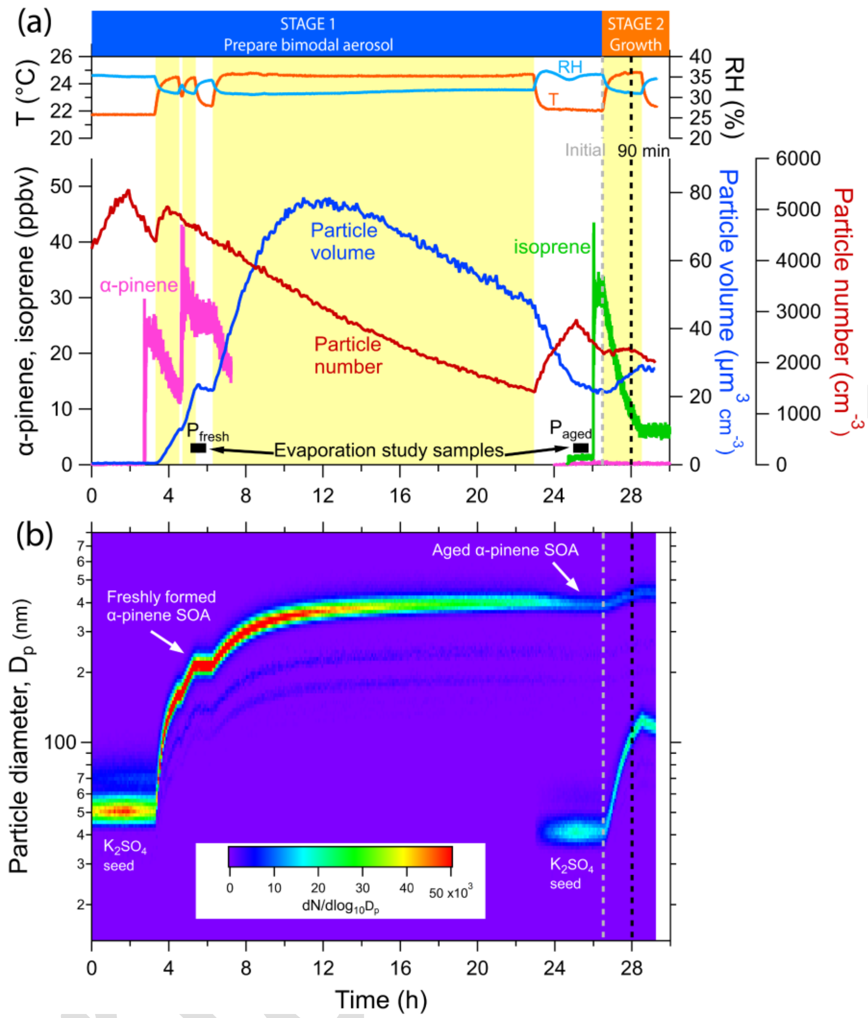

Figure 1. Observed time evolutions of key variables in experiment 1. (a) Time records of temperature (T), relative humidity (RH), α-pinene, isoprene, particle volume and number concentrations in the large environmental chamber as a function of time. In stage 1, a bimodal aerosol consisting of Aitken mode potassium sulfate particles (mode diameter ~40 nm) and accumulation mode α-pinene SOA particles (mode diameter ~385.4 nm) was prepared in the chamber. The yellow shading indicates the periods when the UV lights in the chamber were turned on. The rapid decrease in the particle volume concentration seen after turning the UV lights off in stage 1 was due to deliberate dilution of chamber air with clean air to adjust the particle concentration to the desired level. Aitken mode particles and isoprene were injected into the chamber toward the end of stage 1. Collection times of freshly formed (P_{fresh}) and aged α-pinene SOA (P_{aged}) samples for evaporation study are indicated with filled black rectangles. In stage 2, the bimodal aerosol grew due to isoprene SOA formation. The gray and black vertical dashed lines represent the conditions at the beginning of stage 2 and after 90 min, respectively. The corresponding aerosol size distributions are shown in (b).

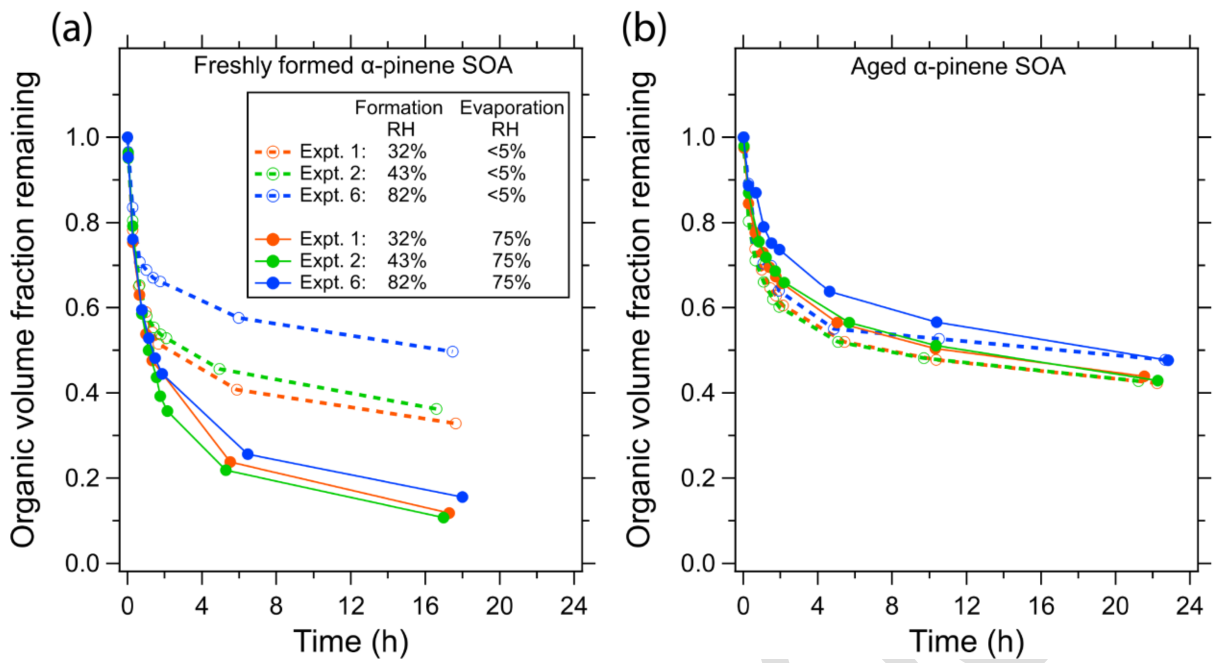

Figure 2. Evaporation kinetics of the accumulation mode α-pinene SOA formed at RH = 32% (orange), RH = 43% (green) and RH = 82% (blue) and evaporated at RH < 5% (open circles) and RH = 75% (filled circles). (a) Volume fraction remaining (VFR) for freshly formed SOA particles sampled within 1.5 to 3 h. (b) VFR for aged SOA particles sampled after ~16 h of photochemical aging. The lines are added to guide the eye.

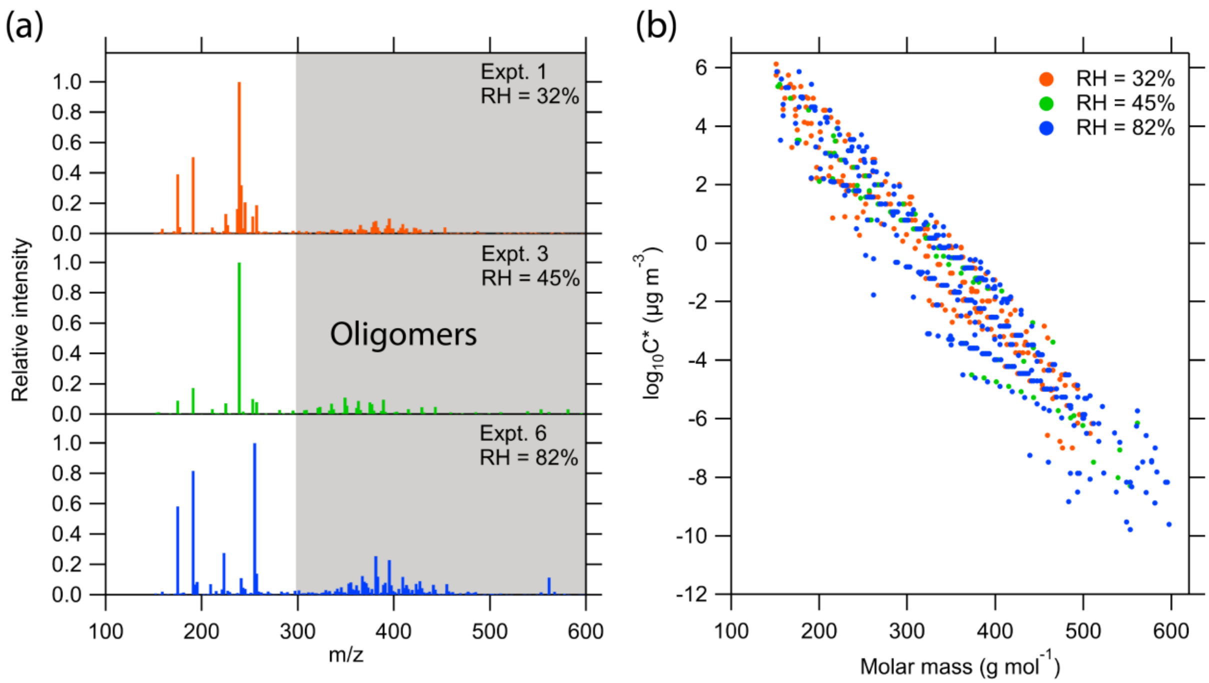

Figure 3. SOA composition and volatility. (a) Nano-DESI-HRMS spectra of bulk SOA samples collected at the end of three experiments conducted at different RH levels. The SOA was composed of a mixture of aged α-pinene SOA and freshly formed isoprene SOA. The m/z peaks in the gray shaded area indicate high molecular weight oligomers formed from particle-phase reactions of smaller monomers. (b) Volatility of SOA species as a function of molar mass as estimated with the molecular corridor approach[59].

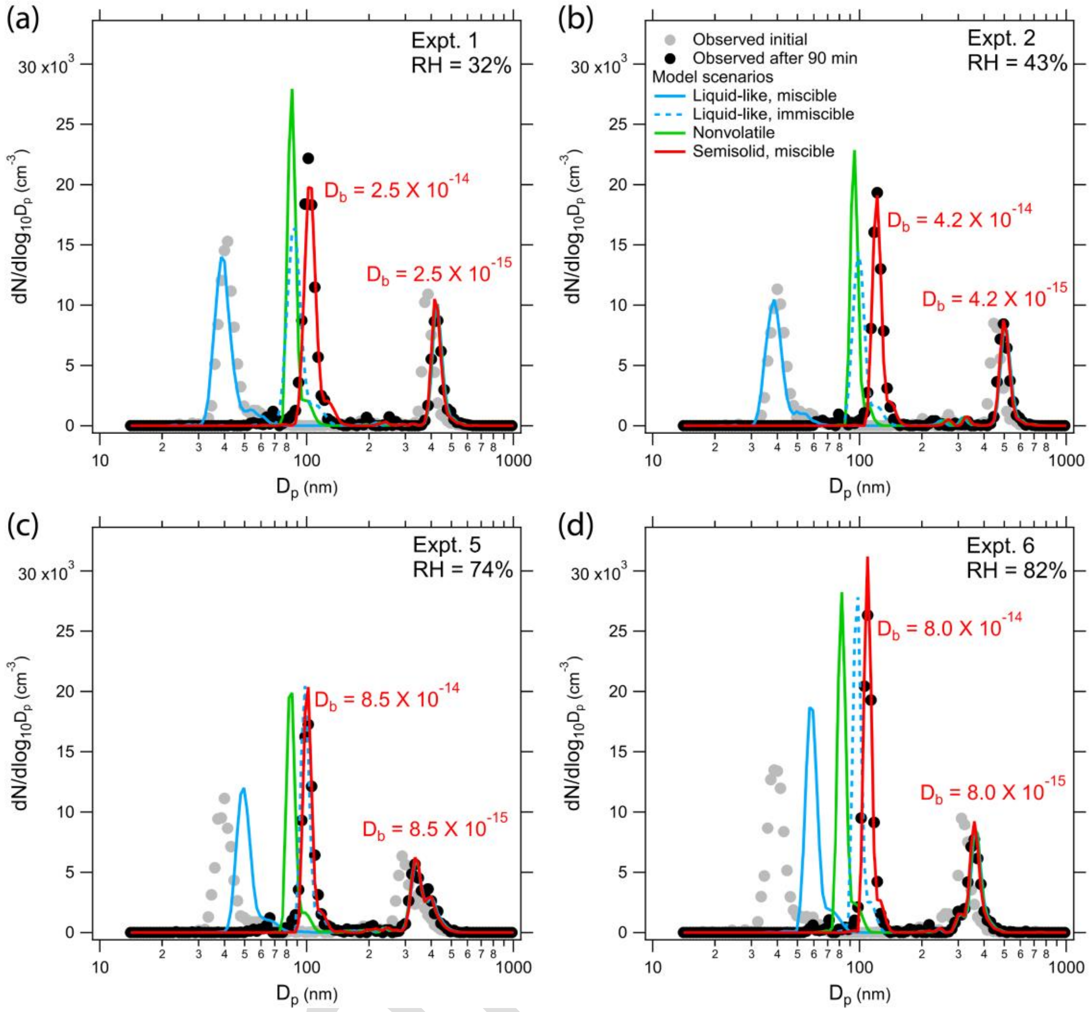

Figure 4. Comparison of the observed and predicted aerosol size distribution evolution due to isoprene SOA formation during stage 2 of four experiments conducted at different RH levels ranging from 32% to 82%. Filled gray circles represent the observed initial bimodal aerosol size distributions consisting of Aitken mode (Dp = ~40 nm) composed of solid potassium sulfate particles and accumulation mode (Dp > 200 nm) composed of aged α-pinene SOA. Filled black circles represent the observed size distribution after growth due to isoprene SOA formation. The colored lines represent model predictions for four different scenarios. Both liquid-like scenarios assume $D_b > 10^{-10}$ cm^2 s^{-1} while the nonvolatile scenario assumes isoprene SOA is formed from condensation of a nonvolatile vapor. None of the scenarios except the semisolid scenario appears to successfully reproduce the growth of both the Aitken and accumulation modes for all the RH levels considered. The D_b values required for the two aerosol modes in the semisolid scenarios are indicated in each panel.

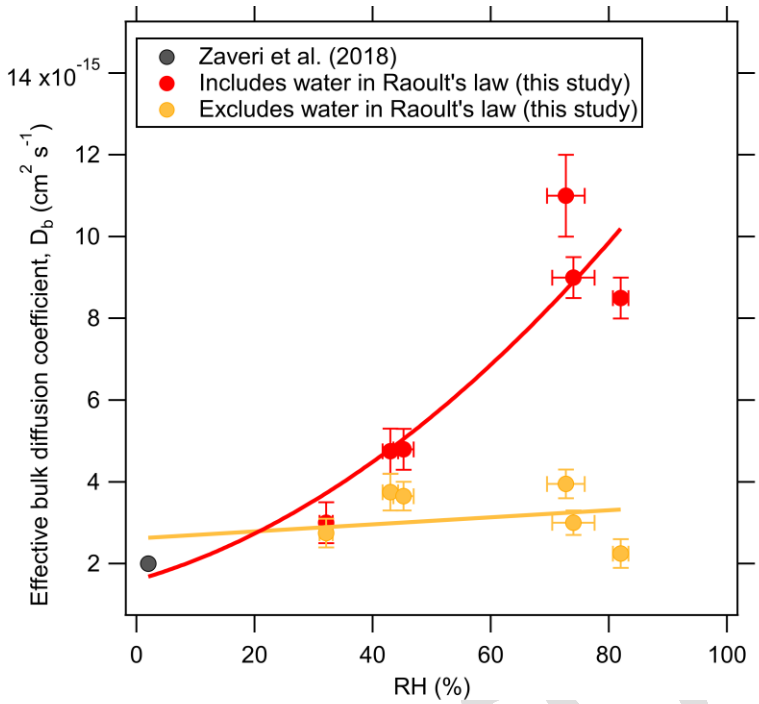

Figure 5. Variation of the model-estimated effective bulk diffusivities for aged α-pinene SOA as a function of RH. Filled red circles represent estimates derived by including the predicted aerosol liquid water as a solvent in Raoult's law calculations in the model. Filled orange circles represent estimates derived by excluding water in Raoult's law. The horizontal error bars represent the standard deviation to the average RH and the vertical error bars represent the range of D_b values obtained with the volatility sensitivity simulations. The red line is a quadratic fit and the orange line is a linear fit to the respective data.

ASSOCIATED CONTENT

Supporting Information. Detailed information on mass spectrometers and box model; schematic of experiment set up; sensitivity of growth kinetics to the prescribed bulk diffusivity values for the Aitken and accumulation modes; sensitivity of growth kinetics to the prescribed mass accommodation coefficient values.

AUTHOR INFORMATION

Corresponding Author

*Phone: 206-528-3215; email: rahul.zaveri@pnnl.gov

Present Addresses

[§]JUUL Labs, San Francisco, CA 94107, USA

‡Laboratory of Atmospheric Chemistry, Paul Scherrer Institute, 5232 Villigen-PSI, Switzerland

[†]Center for Electron Microscopy and Analysis, The Ohio State University, Columbus, OH 43212, USA

Notes

The authors declare no competing financial interest

ACKNOWLEDGMENTS

This research was supported by the Office of Science of the U.S. Department of Energy (DOE) as part of the Atmospheric System Research (ASR) program and by the Environmental Molecular Sciences Laboratory (EMSL), a national scientific user facility sponsored by the DOE's Office of Biological and Environmental Research at Pacific Northwest National Laboratory (PNNL). PNNL is operated for DOE by Battelle Memorial Institute under contract DE-AC05-76RL01830. Data used in this work are available from the corresponding author (rahul.zaveri@pnnl.gov).

REFERENCES

1. Boucher, O.; Randall, D.; Artaxo, P.; Bretherton, C.; Feingold, G.; Forster, P.; Kerminen, V.-M.; Kondo, Y.; Liao, H.; Lohmann, U.; Rasch, P.; Satheesh, S. K.; Sherwood, S.; Stevens, B.; Zhang, X. Y., Clouds and Aerosols. In *Climate Change 2013: The Physical Science Basis. Contribution of Working Group I to the Fifth Assessment Report of the Intergovernmental Panel on Climate Change*, Stocker, T. F.; Qin, D.; Plattner, G.-K.; Tignor, M.; Allen, S. K.; Boschung, J.; Nauels, A.; Xia, Y.; Bex, V.; Midgley, P. M., Eds. Cambridge University Press: Cambridge, United Kingdom and New York, NY, USA, 2013; pp 571–658.
2. Jimenez, J. L.; Canagaratna, M. R.; Donahue, N. M.; Prevot, A. S.; Zhang, Q.; Kroll, J. H.; DeCarlo, P. F.; Allan, J. D.; Coe, H.; Ng, N. L.; Aiken, A. C.; Docherty, K. S.; Ulbrich, I. M.; Grieshop, A. P.; Robinson, A. L.; Duplissy, J.; Smith, J. D.; Wilson, K. R.; Lanz, V. A.; Hueglin, C.; Sun, Y. L.; Tian, J.; Laaksonen, A.; Raatikainen, T.; Rautiainen, J.; Vaattovaara, P.; Ehn, M.; Kulmala, M.; Tomlinson, J. M.; Collins, D. R.; Cubison, M. J.; Dunlea, E. J.; Huffman, J. A.; Onasch, T. B.; Alfarra, M. R.; Williams, P. I.; Bower, K.; Kondo, Y.; Schneider, J.; Drewnick, F.; Borrmann, S.; Weimer, S.; Demerjian, K.; Salcedo, D.; Cottrell, L.; Griffin, R.; Takami, A.; Miyoshi, T.; Hatakeyama, S.; Shimono, A.; Sun, J. Y.; Zhang, Y. M.; Dzepina, K.; Kimmel, J. R.; Sueper, D.; Jayne, J. T.; Herndon, S. C.; Trimborn, A. M.; Williams, L. R.; Wood, E. C.; Middlebrook, A. M.; Kolb, C. E.; Baltensperger, U.; Worsnop, D. R., Evolution of organic aerosols in the atmosphere. *Science* **2009,** *326*, 1525-1529.
3. Zhang, Q.; Jimenez, J. L.; Canagaratna, M. R.; Allan, J. D.; Coe, H.; Ulbrich, I.; Alfarra, M. R.; Takami, A.; Middlebrook, A. M.; Sun, Y. L.; Dzepina, K.; Dunlea, E.; Docherty, K.; DeCarlo, P. F.; Salcedo, D.; Onasch, T.; Jayne, J. T.; Miyoshi, T.; Shimono, A.; Hatakeyama, S.; Takegawa, N.; Kondo, Y.; Schneider, J.; Drewnick, F.; Borrmann, S.; Weimer, S.; Demerjian, K.; Williams, P.; Bower, K.; Bahreini, R.; Cottrell, L.; Griffin, R. J.; Rautiainen, J.; Sun, J. Y.; Zhang, Y. M.; Worsnop, D. R., Ubiquity and dominance of oxygenated species in organic aerosols in anthropogenically-influenced Northern Hemisphere midlatitudes. *Geophysical Research Letters* **2007,** *34*, L13801.
4. Spracklen, D. V.; Jimenez, J. L.; Carslaw, K. S.; Worsnop, D. R.; Evans, M. J.; Mann, G. W.; Zhang, Q.; Canagaratna, M. R.; Allan, J.; Coe, H.; McFiggans, G.; Rap, A.; Forster, P., Aerosol mass spectrometer constraint on the global secondary organic aerosol budget. *Atmos. Chem. Phys.* **2011,** *11*, (23), 12109-12136.
5. Robinson, A. L.; Donahue, N. M.; Shrivastava, M. K.; Weitkamp, E. A.; Sage, A. M.; Grieshop, A. P.; Lane, T. E.; Pierce, J. R.; Pandis, S. N., Rethinking organic aerosols: semivolatile emissions and photochemical aging. *Science* **2007,** *315*, (5816), 1259-62.
6. Schauer, J. J.; Kleeman, M. J.; Cass, G. R.; Simoneit, B. R. T., Measurement of Emissions from Air Pollution Sources. 2. C1 through C30 Organic Compounds from Medium Duty Diesel Trucks. *Environmental Science & Technology* **1999,** *33*, (10), 1578-1587.
7. Schauer, J. J.; Kleeman, M. J.; Cass, G. R.; Simoneit, B. R. T., Measurement of Emissions from Air Pollution Sources. 5. C1−C32 Organic Compounds from Gasoline-Powered Motor Vehicles. *Environmental Science & Technology* **2002,** *36*, (6), 1169-1180.
8. Guenther, A.; Hewitt, C. N.; Erickson, D.; Fall, R.; Geron, C.; Graedel, T.; Harley, P.; Klinger, L.; Lerdau, M.; McKay, W. A.; Pierce, T.; Scholes, B.; Steinbrecher, R.; Tallamraju, R.; Taylor, J.; Zimmerman, P., A global model of natural volatile organic compound emissions. *Journal of Geophysical Research: Atmospheres* **1995,** *100*, (D5), 8873-8892.

9. Kesselmeier, J.; Staudt, M., Biogenic Volatile Organic Compounds (VOC): An Overview on Emission, Physiology and Ecology. *Journal of Atmospheric Chemistry* **1999,** *33*, (1), 23-88.

10. Lathière, J.; Hauglustaine, D. A.; Friend, A. D.; De Noblet-Ducoudré, N.; Viovy, N.; Folberth, G. A., Impact of climate variability and land use changes on global biogenic volatile organic compound emissions. *Atmos. Chem. Phys.* **2006,** *6*, (8), 2129-2146.

11. Guenther, A. B.; Jiang, X.; Heald, C. L.; Sakulyanontvittaya, T.; Duhl, T.; Emmons, L. K.; Wang, X., The Model of Emissions of Gases and Aerosols from Nature version 2.1 (MEGAN2.1): an extended and updated framework for modeling biogenic emissions. *Geosci. Model Dev.* **2012,** *5*, (6), 1471-1492.

12. Riipinen, I.; Pierce, J. R.; Yli-Juuti, T.; Nieminen, T.; Hakkinen, S.; Ehn, M.; Junninen, H.; Lehtipalo, K.; Petaja, T.; Slowik, J.; Chang, R.; Shantz, N. C.; Abbatt, J.; Leaitch, W. R.; Kerminen, V. M.; Worsnop, D. R.; Pandis, S. N.; Donahue, N. M.; Kulmala, M., Organic condensation: a vital link connecting aerosol formation to cloud condensation nuclei (CCN) concentrations. *Atmospheric Chemistry and Physics* **2011,** *11*, (8), 3865-3878.

13. Riipinen, I.; Yli-Juuti, T.; Pierce, J. R.; Petaja, T.; Worsnop, D. R.; Kulmala, M.; Donahue, N. M., The contribution of organics to atmospheric nanoparticle growth. *Nat Geosci* **2012,** *5*, (7), 453-458.

14. Pierce, J. R.; Leaitch, W. R.; Liggio, J.; Westervelt, D. M.; Wainwright, C. D.; Abbatt, J. P. D.; Ahlm, L.; Al-Basheer, W.; Cziczo, D. J.; Hayden, K. L.; Lee, A. K. Y.; Li, S. M.; Russell, L. M.; Sjostedt, S. J.; Strawbridge, K. B.; Travis, M.; Vlasenko, A.; Wentzell, J. J. B.; Wiebe, H. A.; Wong, J. P. S.; Macdonald, A. M., Nucleation and condensational growth to CCN sizes during a sustained pristine biogenic SOA event in a forested mountain valley. *Atmospheric Chemistry and Physics* **2012,** *12*, (7), 3147-3163.

15. Shiraiwa, M.; Zuend, A.; Bertram, A. K.; Seinfeld, J. H., Gas–particle partitioning of atmospheric aerosols: interplay of physical state, non-ideal mixing and morphology. *Physical Chemistry Chemical Physics* **2013,** *15*, (27), 11441-11453.

16. Zaveri, R. A.; Easter, R. C.; Shilling, J. E.; Seinfeld, J. H., Modeling kinetic partitioning of secondary organic aerosol and size distribution dynamics: representing effects of volatility, phase state, and particle-phase reaction. *Atmospheric Chemistry and Physics* **2014,** *14*, (10), 5153-5181.

17. Shiraiwa, M.; Seinfeld, J. H., Equilibration timescale of atmospheric secondary organic aerosol partitioning. *Geophysical Research Letters* **2012,** *39*, L24801.

18. Fuchs, N. A.; Sutugin, A. G., HIGH-DISPERSED AEROSOLS. In *Topics in Current Aerosol Research*, Hidy, G. M.; Brock, J. R., Eds. Pergamon: 1971; p 1.

19. Zhang, X.; Pandis, S. N.; Seinfeld, J. H., Diffusion-Limited Versus Quasi-Equilibrium Aerosol Growth. *Aerosol Science and Technology* **2012,** *46*, (8), 874-885.

20. Jokinen, T.; Berndt, T.; Makkonen, R.; Kerminen, V.-M.; Junninen, H.; Paasonen, P.; Stratmann, F.; Herrmann, H.; Guenther, A. B.; Worsnop, D. R.; Kulmala, M.; Ehn, M.; Sipilä, M., Production of extremely low volatile organic compounds from biogenic emissions: Measured yields and atmospheric implications. *Proceedings of the National Academy of Sciences* **2015,** *112*, (23), 7123-7128.

21. Pankow, J. F., An absorption model of gas/particle partitioning of organic compounds in the atmosphere. *Atmos. Environ.* **1994,** *28*, (2), 185-188.

22. Scott, C. E.; Spracklen, D. V.; Pierce, J. R.; Riipinen, I.; D'Andrea, S. D.; Rap, A.; Carslaw, K. S.; Forster, P. M.; Artaxo, P.; Kulmala, M.; Rizzo, L. V.; Swietlicki, E.; Mann, G. W.; Pringle, K. J., Impact of gas-to-particle partitioning approaches on the simulated radiative effects of biogenic secondary organic aerosol. *Atmospheric Chemistry and Physics* **2015,** *15*, (22), 12989-13001.

23. Tsigaridis, K.; Daskalakis, N.; Kanakidou, M.; Adams, P. J.; Artaxo, P.; Bahadur, R.; Balkanski, Y.; Bauer, S. E.; Bellouin, N.; Benedetti, A.; Bergman, T.; Berntsen, T. K.; Beukes, J. P.; Bian, H.; Carslaw, K. S.; Chin, M.; Curci, G.; Diehl, T.; Easter, R. C.; Ghan, S. J.; Gong, S. L.; Hodzic, A.; Hoyle, C. R.; Iversen, T.; Jathar, S.; Jimenez, J. L.; Kaiser, J. W.; Kirkevåg, A.; Koch, D.; Kokkola, H.; Lee, Y. H.; Lin, G.; Liu, X.; Luo, G.; Ma, X.; Mann, G. W.; Mihalopoulos, N.; Morcrette, J. J.; Müller, J. F.; Myhre, G.; Myriokefalitakis, S.; Ng, N. L.; O'Donnell, D.; Penner, J. E.; Pozzoli, L.; Pringle, K. J.; Russell, L. M.; Schulz, M.; Sciare, J.; Seland, Ø.; Shindell,

D. T.; Sillman, S.; Skeie, R. B.; Spracklen, D.; Stavrakou, T.; Steenrod, S. D.; Takemura, T.; Tiitta, P.; Tilmes, S.; Tost, H.; van Noije, T.; van Zyl, P. G.; von Salzen, K.; Yu, F.; Wang, Z.; Wang, Z.; Zaveri, R. A.; Zhang, H.; Zhang, K.; Zhang, Q.; Zhang, X., The AeroCom evaluation and intercomparison of organic aerosol in global models. *Atmos. Chem. Phys.* **2014,** *14*, (19), 10845-10895.

24. Virtanen, A.; Joutsensaari, J.; Koop, T.; Kannosto, J.; Yli-Pirila, P.; Leskinen, J.; Makela, J. M.; Holopainen, J. K.; Poschl, U.; Kulmala, M.; Worsnop, D. R.; Laaksonen, A., An amorphous solid state of biogenic secondary organic aerosol particles. *Nature* **2010,** *467*, (7317), 824-827.

25. Vaden, T. D.; Imre, D.; Beranek, J.; Shrivastava, M.; Zelenyuk, A., Evaporation kinetics and phase of laboratory and ambient secondary organic aerosol. *Proceedings of the National Academy of Sciences of the United States of America* **2011,** *108*, (6), 2190-2195.

26. Saukko, E.; Lambe, A. T.; Massoli, P.; Koop, T.; Wright, J. P.; Croasdale, D. R.; Pedernera, D. A.; Onasch, T. B.; Laaksonen, A.; Davidovits, P.; Worsnop, D. R.; Virtanen, A., Humidity-dependent phase state of SOA particles from biogenic and anthropogenic precursors. *Atmospheric Chemistry and Physics* **2012,** *12*, (16), 7517-7529.

27. Renbaum-Wolff, L.; Grayson, J. W.; Bateman, A. P.; Kuwata, M.; Sellier, M.; Murray, B. J.; Shilling, J. E.; Martin, S. T.; Bertram, A. K., Viscosity of alpha-pinene secondary organic material and implications for particle growth and reactivity. *Proceedings of the National Academy of Sciences of the United States of America* **2013,** *110*, (20), 8014-8019.

28. Kidd, C.; Perraud, V.; Wingen, L. M.; Finlayson-Pitts, B. J., Integrating phase and composition of secondary organic aerosol from the ozonolysis of alpha-pinene. *Proceedings of the National Academy of Sciences of the United States of America* **2014,** *111*, (21), 7552-7557.

29. Hawkins, L. N.; Baril, M. J.; Sedehi, N.; Galloway, M. M.; De Haan, D. O.; Schill, G. P.; Tolbert, M. A., Formation of semisolid, oligomerized aqueous SOA: Lab simulations of cloud Processing. *Environmental Science & Technology* **2014,** *48*, (4), 2273-2280.

30. Song, M. J.; Liu, P. F. F.; Hanna, S. J.; Zaveri, R. A.; Potter, K.; You, Y.; Martin, S. T.; Bertram, A. K., Relative humidity-dependent viscosity of secondary organic material from toluene photo-oxidation and possible implications for organic particulate matter over megacities. *Atmospheric Chemistry and Physics* **2016,** *16*, (14), 8817-8830.

31. Bateman, A. P.; Gong, Z. H.; Harder, T. H.; de Sa, S. S.; Wang, B. B.; Castillo, P.; China, S.; Liu, Y. J.; O'Brien, R. E.; Palm, B. B.; Shiu, H. W.; Cirino, G. G.; Thalman, R.; Adachi, K.; Alexander, M. L.; Artaxo, P.; Bertram, A. K.; Buseck, P. R.; Gilles, M. K.; Jimenez, J. L.; Laskin, A.; Manzi, A. O.; Sedlacek, A.; Souza, R. A. F.; Wang, J.; Zaveri, R.; Martin, S. T., Anthropogenic influences on the physical state of submicron particulate matter over a tropical forest. *Atmospheric Chemistry and Physics* **2017,** *17*, (3), 1759-1773.

32. Bateman, A. P.; Gong, Z. H.; Liu, P. F.; Sato, B.; Cirino, G.; Zhang, Y.; Artaxo, P.; Bertram, A. K.; Manzi, A. O.; Rizzo, L. V.; Souza, R. A. F.; Zaveri, R. A.; Martin, S. T., Sub-micrometre particulate matter is primarily in liquid form over Amazon rainforest. *Nat Geosci* **2016,** *9*, (1), 34-+.

33. Grayson, J. W.; Zhang, Y.; Mutzel, A.; Renbaum-Wolff, L.; Boge, O.; Kamal, S.; Herrmann, H.; Martin, S. T.; Bertram, A. K., Effect of varying experimental conditions on the viscosity of alpha-pinene derived secondary organic material. *Atmospheric Chemistry and Physics* **2016,** *16*, (10), 6027-6040.

34. Zaveri, R. A.; Shilling, J. E.; Zelenyuk, A.; Liu, J. M.; Bell, D. M.; D'Ambro, E. L.; Gaston, C.; Thornton, J. A.; Laskin, A.; Lin, P.; Wilson, J.; Easter, R. C.; Wang, J.; Bertram, A. K.; Martin, S. T.; Seinfeld, J. H.; Worsnop, D. R., Growth Kinetics and Size Distribution Dynamics of Viscous Secondary Organic Aerosol. *Environmental Science & Technology* **2018,** *52*, (3), 1191-1199.

35. Song, M.; Liu, P. F.; Hanna, S. J.; Li, Y. J.; Martin, S. T.; Bertram, A. K., Relative humidity-dependent viscosities of isoprene-derived secondary organic material and atmospheric implications for isoprene-dominant forests. *Atmos. Chem. Phys.* **2015,** *15*, (9), 5145-5159.

36. Bateman, A. P.; Bertram, A. K.; Martin, S. T., Hygroscopic Influence on the Semisolid-to-Liquid Transition of Secondary Organic Materials. *The Journal of Physical Chemistry A* **2015,** *119*, (19), 4386-4395.

37. Hosny, N. A.; Fitzgerald, C.; Vyšniauskas, A.; Athanasiadis, A.; Berkemeier, T.; Uygur, N.; Pöschl, U.; Shiraiwa, M.; Kalberer, M.; Pope, F. D.; Kuimova, M. K., Direct imaging of changes in aerosol particle viscosity upon hydration and chemical aging. *Chem. Sci.* **2016,** *7*, (2), 1357-1367.
38. Wilson, J.; Imre, D.; Beránek, J.; Shrivastava, M.; Zelenyuk, A., Evaporation Kinetics of Laboratory-Generated Secondary Organic Aerosols at Elevated Relative Humidity. *Environmental Science & Technology* **2015,** *49*, (1), 243-249.
39. O'Brien, R. E.; Neu, A.; Epstein, S. A.; MacMillan, A. C.; Wang, B.; Kelly, S. T.; Nizkorodov, S. A.; Laskin, A.; Moffet, R. C.; Gilles, M. K., Physical properties of ambient and laboratory-generated secondary organic aerosol. *Geophysical Research Letters* **2014,** *41*, (12), 4347-4353.
40. Heaton, K. J.; Dreyfus, M. A.; Wang, S.; Johnston, M. V., Oligomers in the early stage of biogenic secondary organic aerosol formation and growth. *Environmental Science & Technology* **2007,** *41*, (17), 6129-6136.
41. Kalberer, M.; Paulsen, D.; Sax, M.; Steinbacher, M.; Dommen, J.; Prevot, A. S. H.; Fisseha, R.; Weingartner, E.; Frankevich, V.; Zenobi, R.; Baltensperger, U., Identification of polymers as major components of atmospheric organic aerosols. *Science* **2004,** *303*, (5664), 1659-1662.
42. Nguyen, T. B.; Laskin, J.; Laskin, A.; Nizkorodov, S. A., Nitrogen-Containing Organic Compounds and Oligomers in Secondary Organic Aerosol Formed by Photooxidation of Isoprene. *Environmental Science & Technology* **2011,** *45*, (16), 6908-6918.
43. Tolocka, M. P.; Jang, M.; Ginter, J. M.; Cox, F. J.; Kamens, R. M.; Johnston, M. V., Formation of Oligomers in Secondary Organic Aerosol. *Environ. Sci. Technol.* **2004,** *38*, 1428-1434.
44. Zhao, Y.; Wingen, L. M.; Perraud, V.; Finlayson-Pitts, B. J., Phase, composition, and growth mechanism for secondary organic aerosol from the ozonolysis of α-cedrene. *Atmos. Chem. Phys.* **2016,** *16*, (5), 3245-3264.
45. Abramson, E.; Imre, D.; Beranek, J.; Wilson, J.; Zelenyuk, A., Experimental determination of chemical diffusion within secondary organic aerosol particles. *Physical Chemistry Chemical Physics* **2013,** *15*, (8), 2983-2991.
46. Yli-Juuti, T.; Pajunoja, A.; Tikkanen, O.-P.; Buchholz, A.; Faiola, C.; Väisänen, O.; Hao, L.; Kari, E.; Peräkylä, O.; Garmash, O.; Shiraiwa, M.; Ehn, M.; Lehtinen, K.; Virtanen, A., Factors controlling the evaporation of secondary organic aerosol from α-pinene ozonolysis. *Geophysical Research Letters* **2017,** *44*, (5), 2562-2570.
47. Zhou, S.; Shiraiwa, M.; McWhinney, R. D.; Pöschl, U.; Abbatt, J. P. D., Kinetic limitations in gas-particle reactions arising from slow diffusion in secondary organic aerosol. *Faraday Discussions* **2013,** *165*, (0), 391-406.
48. Li, Y.; Shiraiwa, M., Timescales of secondary organic aerosols to reach equilibrium at various temperatures and relative humidities. *Atmos. Chem. Phys.* **2019,** *19*, (9), 5959-5971.
49. Liu, P.; Li, Y. J.; Wang, Y.; Gilles, M. K.; Zaveri, R. A.; Bertram, A. K.; Martin, S. T., Lability of secondary organic particulate matter. *Proceedings of the National Academy of Sciences* **2016,** *113*, (45), 12643.
50. Ye, Q.; Robinson, E. S.; Ding, X.; Ye, P.; Sullivan, R. C.; Donahue, N. M., Mixing of secondary organic aerosols versus relative humidity. *Proceedings of the National Academy of Sciences* **2016,** *113*, (45), 12649.
51. Liu, S.; Shilling, J. E.; Song, C.; Hiranuma, N.; Zaveri, R. A.; Russell, L. M., Hydrolysis of organonitrate functional groups in aerosol particles. *Aerosol Science and Technology* **2012,** *46*, (12), 1359-1369.
52. Freney, E. J.; Martin, S. T.; Buseck, P. R., Deliquescence and Efflorescence of Potassium Salts Relevant to Biomass-Burning Aerosol Particles. *Aerosol Science and Technology* **2009,** *43*, (8), 799-807.
53. Lindinger, W.; Hansel, A.; Jordan, A., On-line monitoring of volatile organic compounds at pptv levels by means of proton-transfer-reaction mass spectrometry (PTR-MS) - Medical applications, food control and environmental research. *International Journal of Mass Spectrometry* **1998,** *173*, (3), 191-241.

54. Roach, P. J.; Laskin, J.; Laskin, A., Nanospray desorption electrospray ionization: an ambient method for liquid-extraction surface sampling in mass spectrometry. *Analyst* **2010,** *135*, (9), 2233-2236.
55. Roach, P. J.; Laskin, J.; Laskin, A., Molecular Characterization of Organic Aerosols Using Nanospray-Desorption/Electrospray Ionization-Mass Spectrometry. *Analytical Chemistry* **2010,** *82*, (19), 7979-7986.
56. Zelenyuk, A.; Imre, D.; Wilson, J.; Zhang, Z.; Wang, J.; Mueller, K., Airborne Single Particle Mass Spectrometers (SPLAT II & miniSPLAT) and New Software for Data Visualization and Analysis in a Geo-Spatial Context. *Journal of The American Society for Mass Spectrometry* **2015,** *26*, (2), 257-270.
57. Zaveri, R. A.; Easter, R. C.; Fast, J. D.; Peters, L. K., Model for Simulating Aerosol Interactions and Chemistry (MOSAIC). *Journal of Geophysical Research-Atmospheres* **2008,** *113*, D13204.
58. Roach, P. J.; Laskin, J.; Laskin, A., Higher-Order Mass Defect Analysis for Mass Spectra of Complex Organic Mixtures. *Analytical Chemistry* **2011,** *83*, (12), 4924-4929.
59. Li, Y.; Pöschl, U.; Shiraiwa, M., Molecular corridors and parameterizations of volatility in the chemical evolution of organic aerosols. *Atmos. Chem. Phys.* **2016,** *16*, (5), 3327-3344.
60. Carlton, A. G.; Wiedinmyer, C.; Kroll, J. H., A review of Secondary Organic Aerosol (SOA) formation from isoprene. *Atmos. Chem. Phys.* **2009,** *9*, (14), 4987-5005.
61. D'Ambro, E. L.; Lee, B. H.; Liu, J. M.; Shilling, J. E.; Gaston, C. J.; Lopez-Hilfiker, F. D.; Schobesberger, S.; Zaveri, R. A.; Mohr, C.; Lutz, A.; Zhang, Z. F.; Gold, A.; Surratt, J. D.; Rivera-Rios, J. C.; Keutsch, F. N.; Thornton, J. A., Molecular composition and volatility of isoprene photochemical oxidation secondary organic aerosol under low- and high-NOx conditions. *Atmospheric Chemistry and Physics* **2017,** *17*, (1), 159-174.
62. Liu, J. M.; D'Ambro, E. L.; Lee, B. H.; Lopez-Hilfiker, F. D.; Zaveri, R. A.; Rivera-Rios, J. C.; Keutsch, F. N.; Iyer, S.; Kurten, T.; Zhang, Z. F.; Gold, A.; Surratt, J. D.; Shilling, J. E.; Thornton, J. A., Efficient Isoprene Secondary Organic Aerosol Formation from a Non-IEPOX Pathway. *Environmental Science & Technology* **2016,** *50*, (18), 9872-9880.
63. Krechmer, J. E.; Coggon, M. M.; Massoli, P.; Nguyen, T. B.; Crounse, J. D.; Hu, W.; Day, D. A.; Tyndall, G. S.; Henze, D. K.; Rivera-Rios, J. C.; Nowak, J. B.; Kimmel, J. R.; Mauldin, R. L.; Stark, H.; Jayne, J. T.; Sipilä, M.; Junninen, H.; Clair, J. M. S.; Zhang, X.; Feiner, P. A.; Zhang, L.; Miller, D. O.; Brune, W. H.; Keutsch, F. N.; Wennberg, P. O.; Seinfeld, J. H.; Worsnop, D. R.; Jimenez, J. L.; Canagaratna, M. R., Formation of low volatility organic compounds and secondary organic aerosol from isoprene hydroxyhydroperoxide low-NO oxidation. *Environmental Science & Technology* **2015,** *49*, (17), 10330-10339.
64. Shiraiwa, M.; Yee, L. D.; Schilling, K. A.; Loza, C. L.; Craven, J. S.; Zuend, A.; Ziemann, P. J.; Seinfeld, J. H., Size distribution dynamics reveal particle-phase chemistry in organic aerosol formation. *Proceedings of the National Academy of Sciences of the United States of America* **2013,** *110*, (29), 11746-11750.
65. Pajunoja, A.; Lambe, A. T.; Hakala, J.; Rastak, N.; Cummings, M. J.; Brogan, J. F.; Hao, L.; Paramonov, M.; Hong, J.; Prisle, N. L.; Malila, J.; Romakkaniemi, S.; Lehtinen, K. E. J.; Laaksonen, A.; Kulmala, M.; Massoli, P.; Onasch, T. B.; Donahue, N. M.; Riipinen, I.; Davidovits, P.; Worsnop, D. R.; Petäjä, T.; Virtanen, A., Adsorptive uptake of water by semisolid secondary organic aerosols. *Geophysical Research Letters* **2015,** *42*, (8), 3063-3068.
66. Rastak, N.; Pajunoja, A.; Acosta Navarro, J. C.; Ma, J.; Song, M.; Partridge, D. G.; Kirkevåg, A.; Leong, Y.; Hu, W. W.; Taylor, N. F.; Lambe, A.; Cerully, K.; Bougiatioti, A.; Liu, P.; Krejci, R.; Petäjä, T.; Percival, C.; Davidovits, P.; Worsnop, D. R.; Ekman, A. M. L.; Nenes, A.; Martin, S.; Jimenez, J. L.; Collins, D. R.; Topping, D. O.; Bertram, A. K.; Zuend, A.; Virtanen, A.; Riipinen, I., Microphysical explanation of the RH-dependent water affinity of biogenic organic aerosol and its importance for climate. *Geophysical Research Letters* **2017,** *44*, (10), 5167-5177.
67. Price, H. C.; Mattsson, J.; Zhang, Y.; Bertram, A. K.; Davies, J. F.; Grayson, J. W.; Martin, S. T.; O'Sullivan, D.; Reid, J. P.; Rickards, A. M. J.; Murray, B. J., Water diffusion in atmospherically relevant alpha-pinene secondary organic material. *Chem. Sci.* **2015,** *6*, (8), 4876-4883.

68. Koop, T.; Bookhold, J.; Shiraiwa, M.; Pöschl, U., Glass transition and phase state of organic compounds: dependency on molecular properties and implications for secondary organic aerosols in the atmosphere. *Physical Chemistry Chemical Physics* **2011,** *13*, (43), 19238-19255.

69. Vander Wall, A. C.; Perraud, V.; Wingen, L. M.; Finlayson-Pitts, B. J., Evidence for a kinetically controlled burying mechanism for growth of high viscosity secondary organic aerosol. *Environmental Science: Processes & Impacts* **2020**.

70. Zhou, S.; Hwang, B. C. H.; Lakey, P. S. J.; Zuend, A.; Abbatt, J. P. D.; Shiraiwa, M., Multiphase reactivity of polycyclic aromatic hydrocarbons is driven by phase separation and diffusion limitations. *Proceedings of the National Academy of Sciences* **2019,** *116*, (24), 11658.

71. Bell, D. M.; Imre, D.; Martin, S. T.; Zelenyuk, A., The properties and behavior of alpha-pinene secondary organic aerosol particles exposed to ammonia under dry conditions. *Physical Chemistry Chemical Physics* **2017,** *19*, (9), 6497-6507.

72. Liu, X.; Day, D. A.; Krechmer, J. E.; Brown, W.; Peng, Z.; Ziemann, P. J.; Jimenez, J. L., Direct measurements of semi-volatile organic compound dynamics show near-unity mass accommodation coefficients for diverse aerosols. *Communications Chemistry* **2019,** *2*, (1), 98.

Supporting Information for:

Particle-phase diffusion modulates partitioning of semivolatile organic compounds to aged secondary organic aerosol

Rahul A. Zaveri, [1,*] *John E. Shilling,* [1] *Alla Zelenyuk,* [1] *Maria A. Zawadowicz,* [1] *Kaitlyn Suski,* [1,§]

Swarup China, [2] *David M. Bell* [1,‡], *Daniel Veghte,* [2,†] *and Alexander Laskin* [3]

[1]Atmospheric Sciences and Global Change Division, Pacific Northwest National Laboratory, Richland, WA 99352, United States

[2]William R. Wiley Environmental Molecular Sciences Laboratory, Pacific Northwest National Laboratory, Richland, WA 99352, United States

[3]Department of Chemistry, Purdue University, West Lafayette, IN 47907, United States

*Correspondence to: R. A. Zaveri (rahul.zaveri@pnnl.gov)

This file includes:

Pages S1-S8
Materials and Methods
Figures S1-S3
References

MATERIALS AND METHODS

Instruments

Single particle mass spectrometer miniSPLAT

A single particle mass spectrometer, miniSPLAT, was used for real-time characterization of particle vacuum aerodynamic diameter (D_{va}), density, shape, and composition. A detailed description of miniSPLAT and its application to quantify room-temperature evaporation kinetics of size-selected particles are provided elsewhere.[1-3] Briefly, individual aerosol particles, sampled into miniSPLAT through an aerodynamic lens inlet are detected by light scattering in two optical stages 10.9 cm apart.[3] The particle time-of-flight between the two optical stages yields particle velocity, which is used to calculate particle D_{va} with precision and accuracy of ±0.5%. The dual particle detection is also used to generate a trigger for the excimer laser, used o generate positive and negative ions and acquire single particle mass spectra. Measurements conducted on size- or mass-selected particles provide information on particle shape, precise density (±0.5%), and evaporation kinetics.

Nano-DESI-HRMS

Off-line filter samples were collected on membrane filters (TE36, Whatman, 0.45 µm pore size) using a four-stage cascade impactor (Sioutas Personal Cascade Impactor, SKC). Samples were collected on stages C and D (particle cut-off sizes: stage C - 0.50 µm, and stage D - 0.25 µm). Samples were deposited along impinging jet streamlines on filter surface. In this way instead of samples scattered around the entire filter, particles were deposited along a line. This sampling method is ideal for probing with the custom-built Nanospray Desorption Electrospray Ionization (Nano-DESI) source coupled to a high resolution LTQ-Orbitrap mass spectrometer (Thermo Electron, Bremen, Germany). Briefly, the sample was placed on a computer-controlled XYZ stage and brought in contact with the Nano-DESI probe, which was assembled using two fused silica capillaries (50 × 185 µm, ID × OD, Polymicro Technologies, L.L.C., Phoenix). A syringe pump at a flow rate of 0.3 µL min^{-1} was used to infuse the solvent (70/30%, acetonitrile/water)[4]. The experiments were typically performed in the positive ionization mode with a resolving power of $m/\Delta m = 10^5$ at m/z 400, with spray voltage of 3.5 kV, and the capillary heated to 250 °C. The instrument was calibrated using a standard calibration MSCAL 5 mixture (Sigma-Aldrich, Inc.) prior to experiments. Mass spectral features with a minimum signal-to-noise ratio of 3 were extracted from the averaged mass spectra of both solvent background and sample using Decon 2LS software [5](http://omics.pnl.gov/software/decontools-decon2ls). HRMS data were processed using a suite of Microsoft Excel macros, including background subtraction, first and second-order mass defect analysis.[6, 7]

Box Model

In this study we used the sectional aerosol box model MOSAIC (Model for Simulating Aerosol Interactions and Chemistry)[8, 9] to interpret the observed aerosol growth kinetics. MOSAIC dynamically partitions multiple compounds to all particle size bins (mean diameter, D_p) by taking into account compound volatility (C^*), gas-phase diffusion (D_g), interfacial mass accommodation (α), intra-particle bulk diffusion (D_b), and reversible particle-phase reactions. In this study, D_g was assumed at 0.05 $cm^2\ s^{-1}$ and $\alpha = 0.1$ for all condensing compounds. The thermodynamic driving force for mass transfer is based on Raoult's law. Bulk diffusion is treated using a combination of (1) an analytical quasi-steady-state treatment for the diffusion–reaction process within the particle phase for fast-reacting organic compounds such that the timescales for their particle-phase concentrations to reach quasi-steady state are shorter than 1 min, and (2) a two-film theory approach for slow- and non-reacting organic compounds. The logarithmically spaced bin structure in the MOSAIC was same as that of the particle size distribution data provided by the SMPS. The number of size bins in the model was set at 120. Transfer of particles between bins due to growth or shrinkage was calculated using a two-moment approach. Coagulation was accounted for in the simulations.

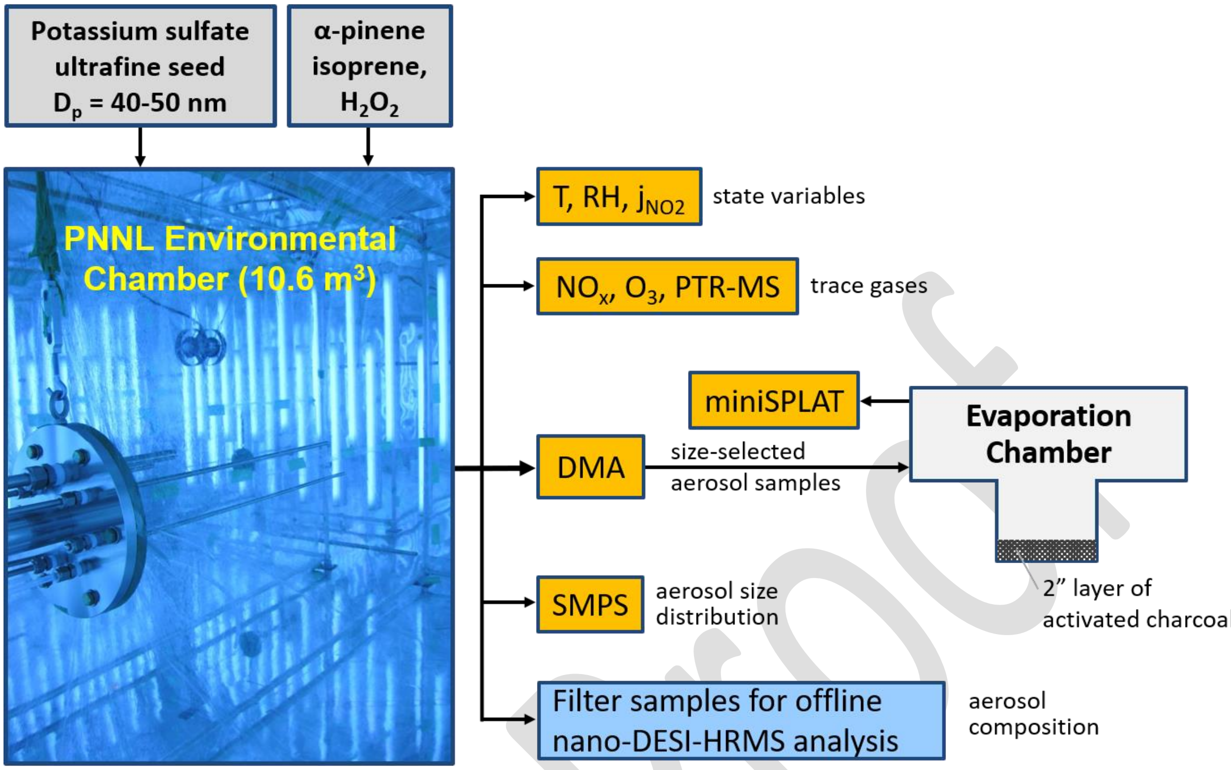

Figure S1. Schematic of experiment set up. Aerosol growth kinetics experiments were conducted in 10.6 m^3 FEP Teflon environmental chamber at Pacific Northwest National Laboratory. The chamber was run in the so-called batch mode where reactants were added to the chamber in discrete quantities. Instruments shown with orange background measured in real time (i.e., online) the state variables, trace gases, particle size distribution. Filter samples were collected at the end of the experiment for offline chemical analysis. Size-selected SOA particles formed in the environmental chamber were transferred at various stages of the experiment into separate small chambers to study their evaporation kinetics at room temperature under dry (RH < 5%) and humid (RH = 75%) conditions.

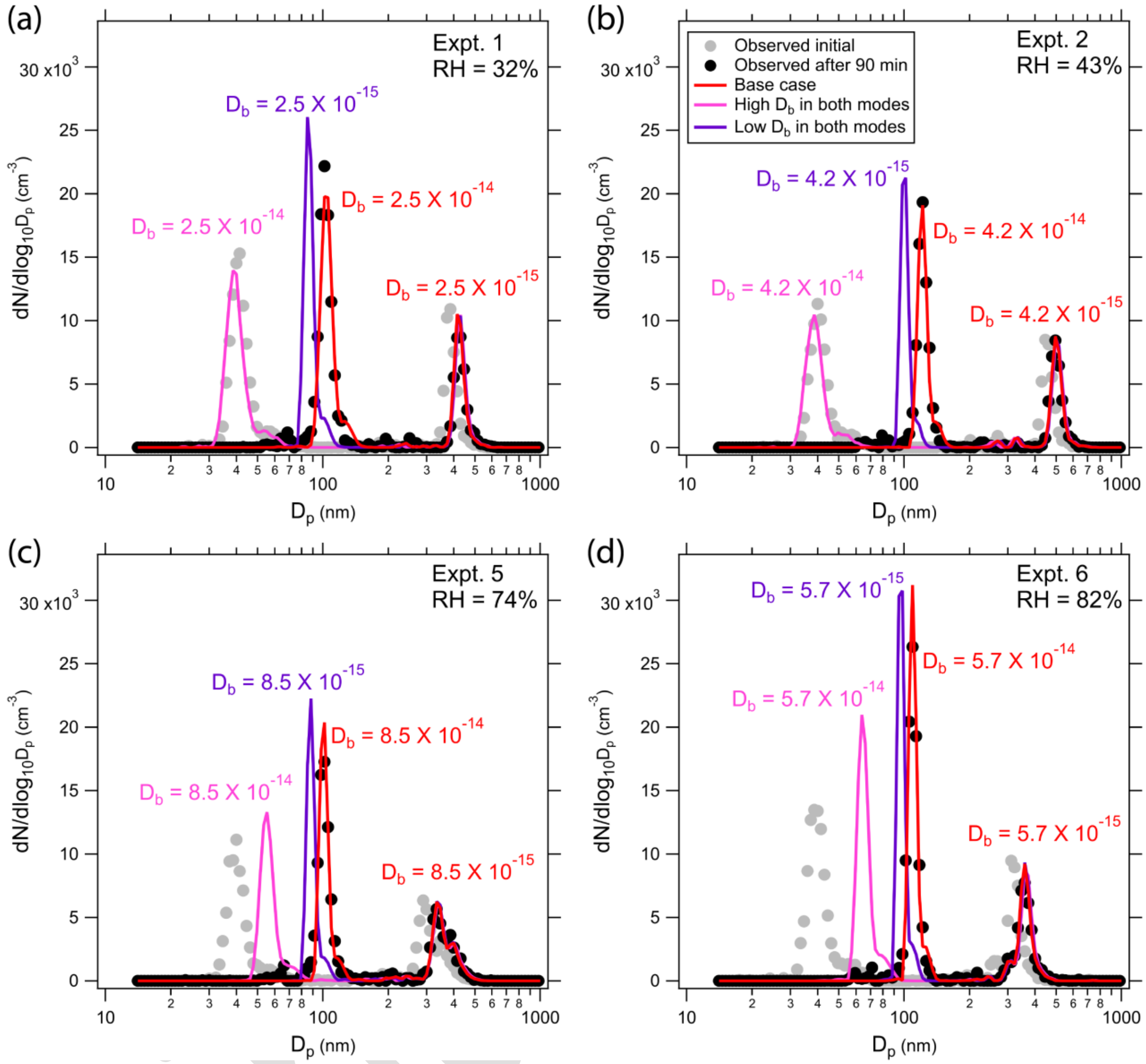

Figure S2. Sensitivity of growth kinetics to the prescribed bulk diffusivity values (cm^2 s^{-1}) for the Aitken and accumulation modes. The base case D_b values (red) are the same as the semisolid scenario shown in Figure 4. In the "high D_b" case, the bulk diffusivity for both aerosol modes is set to the value shown in pink. In the "low D_b" case, the bulk diffusivity for both aerosol modes is set to the value shown in purple.

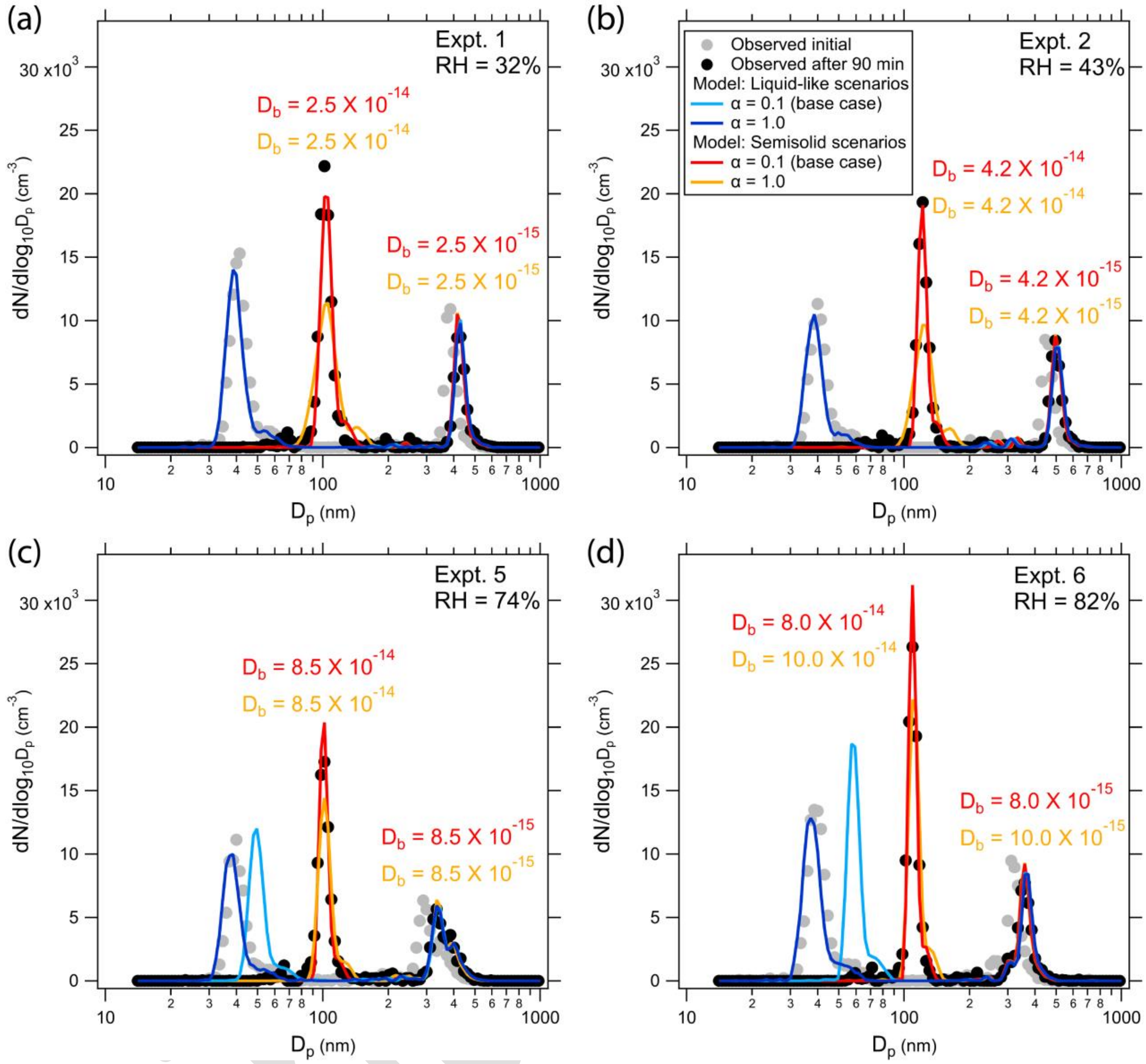

Figure S3. Sensitivity of growth kinetics to the prescribed mass accommodation (α) values for both the Aitken and accumulation modes, assuming isoprene and a-pinene SOA in the accumulation mode are miscible in both liquid-like and semisolid scenarios. The base case scenarios are the same as those shown in Figure 4. The liquid-like scenarios assume $D_b > 10^{-10}$ cm^2 s^{-1}. The D_b values required for the two aerosol modes in the semisolid scenarios are indicated in each panel; the values in red are for the base case (α = 0.1) and the values in orange are for α = 0.1.

.

References

1. Vaden, T. D.; Imre, D.; Beranek, J.; Shrivastava, M.; Zelenyuk, A., Evaporation kinetics and phase of laboratory and ambient secondary organic aerosol. *Proceedings of the National Academy of Sciences of the United States of America* **2011,** *108*, (6), 2190-2195.

2. Wilson, J.; Imre, D.; Beránek, J.; Shrivastava, M.; Zelenyuk, A., Evaporation Kinetics of Laboratory-Generated Secondary Organic Aerosols at Elevated Relative Humidity. *Environmental Science & Technology* **2015,** *49*, (1), 243-249.

3. Zelenyuk, A.; Imre, D.; Wilson, J.; Zhang, Z.; Wang, J.; Mueller, K., Airborne Single Particle Mass Spectrometers (SPLAT II & miniSPLAT) and New Software for Data Visualization and Analysis in a Geo-Spatial Context. *Journal of The American Society for Mass Spectrometry* **2015,** *26*, (2), 257-270.

4. Roach, P. J.; Laskin, J.; Laskin, A., Nanospray desorption electrospray ionization: an ambient method for liquid-extraction surface sampling in mass spectrometry. *Analyst* **2010,** *135*, (9), 2233-2236.

5. Jaitly, N.; Mayampurath, A.; Littlefield, K.; Adkins, J. N.; Anderson, G. A.; Smith, R. D., Decon2LS: An open-source software package for automated processing and visualization of high resolution mass spectrometry data. *BMC Bioinformatics* **2009,** *10*, 87.

6. Eckert, P. A.; Roach, P. J.; Laskin, A.; Laskin, J., Chemical characterization of crude petroleum using nanospray desorption electrospray ionization coupled with high-resolution mass spectrometry. *Anal Chem* **2012,** *84*, (3), 1517-25.

7. Roach, P. J.; Laskin, J.; Laskin, A., Higher-Order Mass Defect Analysis for Mass Spectra of Complex Organic Mixtures. *Analytical Chemistry* **2011,** *83*, (12), 4924-4929.

8. Zaveri, R. A.; Easter, R. C.; Fast, J. D.; Peters, L. K., Model for Simulating Aerosol Interactions and Chemistry (MOSAIC). *Journal of Geophysical Research-Atmospheres* **2008,** *113*, D13204.

9. Zaveri, R. A.; Easter, R. C.; Shilling, J. E.; Seinfeld, J. H., Modeling kinetic partitioning of secondary organic aerosol and size distribution dynamics: representing effects of volatility, phase state, and particle-phase reaction. *Atmospheric Chemistry and Physics* **2014,** *14*, (10), 5153-5181.